

www.acsami.org Research Article

Electrically Enhanced Exchange Bias via Solid-State Magneto-ionics

Peyton D. Murray, Christopher J. Jensen, Alberto Quintana, Junwei Zhang, Xixiang Zhang, Alexander J. Grutter, Brian J. Kirby, and Kai Liu*



Cite This: *ACS Appl. Mater. Interfaces* 2021, 13, 38916–38922



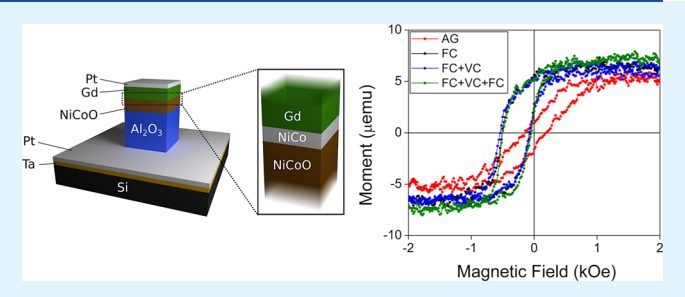
ACCESS

Metrics & More

Article Recommendations

s Supporting Information

ABSTRACT: Electrically induced ionic motion offers a new way to realize voltage-controlled magnetism, opening the door to a new generation of logic, sensor, and data storage technologies. Here, we demonstrate an effective approach to magneto-ionically and electrically tune the exchange bias in $\mathrm{Gd/Ni_{1-x}Co_xO}$ thin films (x=0.50 and 0.67), where neither of the layers alone is ferromagnetic at room temperature. The Gd capping layer deposited onto antiferromagnetic $\mathrm{Ni_{1-x}Co_xO}$ initiates a solid-state redox reaction that reduces an interfacial region of the oxide to ferromagnetic NiCo. An exchange bias is established after field



cooling (FC), which can be enhanced by up to 35% after a voltage conditioning and subsequently reset with a second FC. These effects are caused by the presence of an interfacial ferromagnetic NiCo layer, which further alloys with the Gd layer upon FC and voltage application, as confirmed by electron microscopy and polarized neutron reflectometry studies. These results highlight the viability of the solid-state magneto-ionic approach to achieve electric control of exchange bias, with potential for energy-efficient magneto-ionic devices.

KEYWORDS: magneto-ionics, electric field control of magnetism, exchange bias, electron energy loss spectroscopy, polarized neutron reflectometry

INTRODUCTION

Methods aiming at controlling magnetism using electric fields have attracted significant interest in recent years with the promise of enabling a new generation of nonvolatile, low-dissipation electronics, 1-9 bypassing the Joule heating effect associated with electric currents in conventional systems. In this regard, atomic-scale control of interfaces via ionic migration in solid-state heterostructures $^{6-13}$ as well as electrolyte-based systems $^{2,14-20}$ has emerged as an effective tool to modify materials properties, which can be further controlled by an electric field. To date, a variety of magnetoionically controlled functionalities have been demonstrated, including magnetic anisotropy, ^{7,8,13} antiferromagnetism, ¹² ferromagnetism, ^{9,14,18,20–23} superconductivity, ^{24,25} Dzyaloshinskii-Moriya interaction, spin textures, ²⁶⁻²⁸ and so on. Many of the magneto-ionic studies have focused on the interfacial electrostatic effect, 2,6-8 where the charge build-up across interfaces under an electric field modifies the electronic structures and materials characteristics. Recent studies have also demonstrated that the electrochemical means, where the interface is transformed by an ion-migration-induced chemical reaction, can modify materials properties well beyond the interface. 12,15,21,24,29 For example, the redox reaction at a ferrimagnetic -GdFe/antiferromagnetic (AF)-NiCoO interface has been shown to trigger oxygen ion migration, which is manifested in the exchange-bias effect. 12 Conversely, this magneto-ionic effect offers a new paradigm to explore the

potential for electrical manipulation of exchange bias. As the exchange bias effect is central to spin-valve-type devices such as magnetic tunnel junctions that enable control of magnetic configurations, ^{30–32} electric control of the exchange bias may lead to substantially more energy-efficient switching than using a magnetic field. Indeed, there has been keen interest in exploring the electric switching of the exchange bias, using multiferroics, ^{33,34} memristors, ³⁵ or electrolytes. ¹⁶

In this work, we present an effective approach to magneto-ionically and electrically tune the exchange bias in Gd/Ni_{1-x}Co_xO thin films (x = 0.50, 0.67). Even though neither of the constituents is ferromagnetic (FM) at room temperature, the Gd layer strips oxygen away from the AF Ni_{1-x}Co_xO (referred to as NiCoO), reducing its interface region to a FM layer. A significant exchange bias is established upon field cooling (FC), which can be further enhanced in an electric field and reset by subsequent FC. Electron microscopy and polarized neutron reflectometry (PNR) studies provide direct evidence of the formation of an FM NiCo interfacial layer and

Received: June 15, 2021 Accepted: July 26, 2021 Published: August 4, 2021





reveal microstructural modifications of the interface upon FC and electric field gating. Our approach combines the strong ionic migration induced by the Gd layer with electrical biasing to allow for on-demand modification of the exchange bias, opening up an effective magneto-ionic pathway toward nonvolatile and energy-efficient magnetic switching devices.

Sample Synthesis. Polycrystalline thin-film samples of Gd/Ni_{0.50}Co_{0.50}O (series 1) and Gd/Ni_{0.33}Co_{0.67}O (series 2) were magnetron-sputtered in an ultrahigh vacuum system with a base pressure in the 10^{-6} Pa range. Gd is a strong oxygen getter material^{21,29} and can extract oxygen from deep within an adjacent oxide layer due to its low electron work function,² with a Curie temperature of 292 K.36 The AF NiCoO has a tunable Néel temperature that scales with the composition:³⁷ $T_{\rm N}$ = 408 K for $Ni_{0.50}{\rm Co}_{0.50}{\rm O}$ and 368 K for $Ni_{0.33}{\rm Co}_{0.67}{\rm O}$. ^{12,38} For series 1, a naturally oxidized Si wafer was first sputtercoated with a Ta (1 nm thick) adhesion layer followed by a Pt (10 nm) layer, forming a bottom electrode. The wafer was then removed from the deposition chamber and lithographically patterned into arrays of 7.5 mm \times 7.5 mm squares uncovered by the resist. Subsequently, an insulating layer of Al₂O₃ (170 nm) was radio frequency (RF)-sputtered from an Al₂O₃ target with a working gas consisting of 2% O₂/98% Ar. Next, a layer of Ni_{0.50}Co_{0.50}O (20 nm) was RF-sputtered from a stoichiometrically balanced target under 0.33 Pa of a 15% O₂/85% Ar working gas mixture. Finally, the sample was capped with a Gd layer (20 nm) followed by a layer of Pt (10 nm), with the latter acting both as a top electrode and as a barrier to protect the sample from atmospheric exposure. Except for the NiCoO layer, sputtering was carried out at a gas pressure of 0.67 Pa. After deposition, the sample was washed in acetone to remove the remaining photoresist, exposing the bottom electrode. The final sample structure is illustrated in Figure 1.

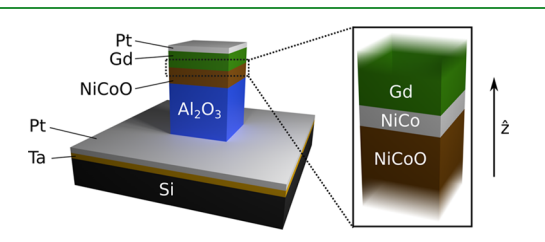


Figure 1. Layer structure of the series 1 samples, with the height of the patterned Al₂O₃/NiCoO/Gd/Pt structures exaggerated. The inset shows a magnified view of the NiCoO/Gd interface, with the emergent metallic NiCo layer explicitly shown. The arrow denotes the $+\hat{z}$ direction.

Series 2 samples were deposited by reactive magnetron sputtering onto thermally oxidized SiO₂ (285 nm) grown on ptype Si, which acts as a bottom electrode. The Ar/O₂ fraction was optimized following reported procedures. 39,40 A Ni_{0.33}Co_{0.67}O (40 nm) layer was then reactively co-sputtered using elemental Ni and Co targets in a 0.33 Pa gas mixture of 6.7% O₂/93.3% Ar at a substrate temperature of 500 °C.⁴¹ Patterned 5 mm \times 5 mm samples were obtained using a mask during the sputtering process. Subsequently, a 20 nm layer of Gd and a 20 nm Pd capping layer were deposited onto the films. This second series was chosen as the exchange bias in Ni_{1-x}Co_xO-based systems is composition-sensitive, due to the competition between the higher T_N of NiO and the larger anisotropy of CoO.42

Magnetometry. Vibrating sample magnetometry measurements of series 1 samples were first carried out in the as-grown (AG) state. A nonzero magnetization is observed, along with a coercivity of 168 Oe (Figure 2a), even though none of the constituent materials alone exhibits ferromagnetism at room temperature. This indicates that a partial reduction of Ni_{0.50}Co_{0.50}O has occurred due to the gettering effect of the Gd layer that leads to an FM layer at the interface, similar to that observed previously in the GdFe/NiCoO system. 12 The equivalent thickness, t, of a continuous FM layer corresponding to the observed moment can be estimated from the saturation magnetization of Ni (495 emu/cm³) $[1 \text{ emu/cm}^3 =$ 1 kA m⁻¹] and Co (1400 emu/cm³), depending on the exact Ni/Co ratio; for these samples, 0.4 nm $\leq t \leq$ 1.3 nm, with the lower and upper bounds determined assuming pure Co and pure Ni, respectively. More details about this layer will be discussed below in the neutron studies.

A second measurement was made after heating the samples in Ar above the Ni_{0.50}Co_{0.50}O T_N to 420 K and then cooling to room temperature in a 10 kOe [1 kOe = 0.1 T/ μ_o] magnetic field. After this FC step, an exchange bias is established with a bias field $H_b = -283$ Oe and an enhanced coercivity of 221 Oe (Figure 2a).

A third measurement was made after a voltage-conditioning (VC) procedure, wherein a 10 V bias (\sim 0.5 MV cm⁻¹ electric field) was applied along the $-\hat{z}$ direction (Figure 1) for 12 h at room temperature, with the O²⁻ ions in the Ni_{0.50}Co_{0.50}O layer expected to drift toward Gd. Magnetometry measurements of this voltage-conditioned (FC + VC) state show an increase in the exchange bias to $H_{\rm b}$ = -308 Oe, along with a further coercivity enhancement to $H_C = 230$ Oe (Figure 2a). Subsequently, a reverse-bias voltage was applied at room temperature using the same 0.5 MV/cm electric field applied for 12 h in the $+\hat{z}$ direction. This reverse-bias voltage conditioned (FC + VC - VC) state showed no appreciable change in the hysteresis loop.

Finally, in a second FC procedure, the sample was again heated to 420 K and then cooled to room temperature in a 10 kOe field. A subsequent magnetometry measurement (FC + VC + FC) shows the major loop returning from the FC + VC state back to the original FC state (Figure 2a), and the electricfield-induced exchange bias is reset.

Magnetometry measurements for series 2 samples were carried out in a superconducting quantum interferometer device magnetometer (MPMS3-Quantum Design), following similar procedures as those for series 1. The AG sample again exhibited an FM-like hysteresis loop, similar to series 1, with a coercivity of H_C = 260 Oe (Figure 2b). Subsequently, a FC process was carried out by increasing the temperature to 400 K, above the $Ni_{0.33}Co_{0.67}O$ T $_{\rm N}$ of 368 K, and cooling down to room temperature in an external field of 10 kOe. An exchange bias of $H_b = -80$ Oe was established, along with an enhanced coercivity of H_C = 276 Oe. This FC sample was then subjected to a voltage gating of 20 V (~0.6 MV/cm) for 12 h. The exchange bias was enhanced to $H_b = -108$ Oe or a 35% increase upon voltage treatment, and the coercivity further increased to 297 Oe. As in series 1 samples, reverse-biasing produced no appreciable effect on the sample, while a second FC procedure can reset the magnetic state of the sample.

Aberration-Corrected Scanning Transmission Electron Microscopy. To further understand the sample microstructure under different conditions, aberration-corrected scanning transmission electron microscopy (Cs-corrected

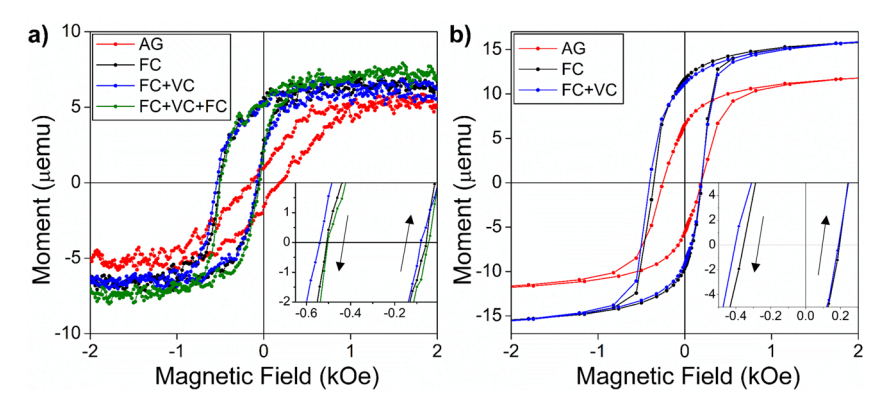


Figure 2. (a) Hysteresis loops of a $Gd/Ni_{0.50}Co_{0.50}O$ sample in the as-grown (AG), after field cooling (FC), after VC (FC + VC), and after a second FC (FC + VC + FC) states. (b) Hysteresis loops of a $Gd/Ni_{0.33}Co_{0.67}O$ sample in the AG, FC, and FC + VC states. Insets show zoomed-in views to highlight the changes in the exchange bias.

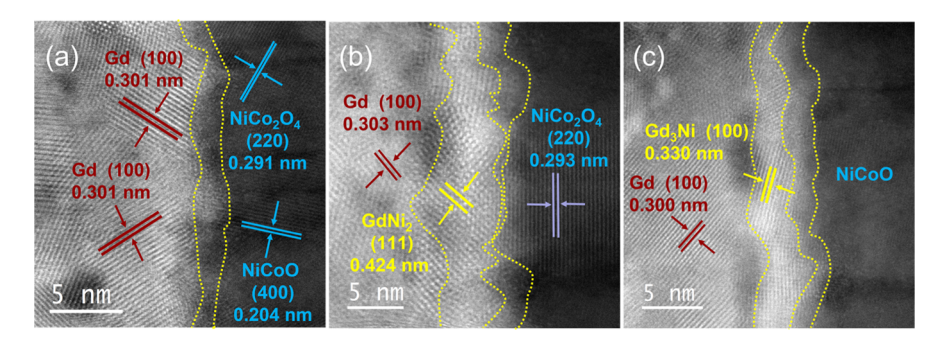


Figure 3. STEM images of the $Gd/Ni_{0.50}Co_{0.50}O$ sample in the (a) AG, (b) FC, and (c) FC + VC states, with Gd and NiCoO on the left and right sides of the interface, respectively. Yellow dashed lines highlight the interface region, including the presence of the crystalline GdNi phase in (b) and (c).

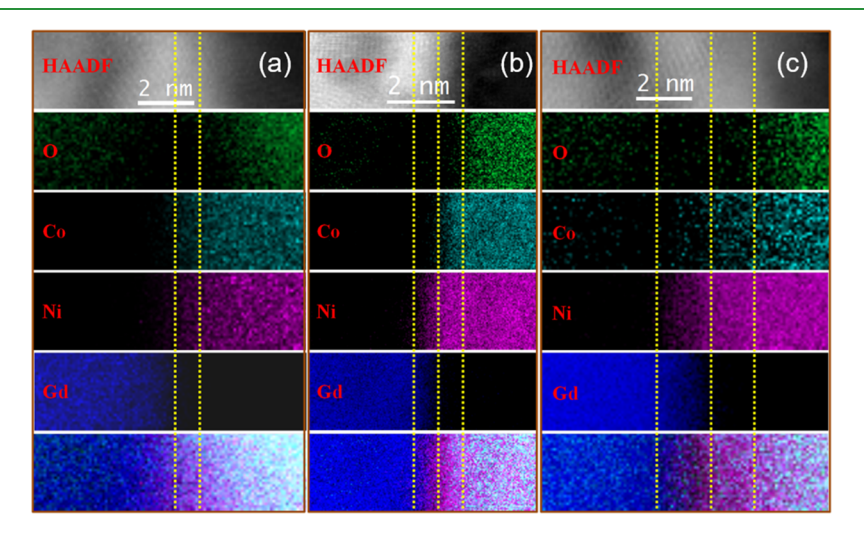


Figure 4. EELS study of the $Gd/Ni_{0.50}Co_{0.50}O$ sample showing elemental distribution maps of Gd (dark blue), Ni (pink), Co (cyan), and O (green) for the (a) AG, (b) FC, and (c) FC + VC states, with the corresponding high-angle annular dark-field (HAADF) image stacked on top. Yellow dashed lines highlight the elemental segregation in the interface region between Gd and NiCoO, showing a CoNi region in (a) and GdNi and CoNi regions in (b) and (c).

STEM) images were acquired at KAUST on three Gd/Ni $_{0.50}$ Co $_{0.50}$ O samples prepared in the AG, FC, and FC + VC states. Representative images of the Gd/Ni $_{0.50}$ Co $_{0.50}$ O interface show small, randomly oriented crystallites identifiable as regions of uniform and parallel lattice fringes, indicating that both Gd and Ni $_{0.50}$ Co $_{0.50}$ O form polycrystalline grains during growth (Figure 3a). Some NiCo $_2$ O $_4$ crystallites are also observed as a result of oxygen leaching from Ni $_{0.50}$ Co $_{0.50}$ O.

After FC, only a few crystal planes are visible; as thermal treatment often improves crystallinity, ²⁰ this increased disorder may be due to disrupted interfaces caused by ionic migration, which is enhanced by the elevated temperatures reached during FC (Figure 3b). Notably, some crystallites of Gd–Ni alloys are observed at the interface region. After VC, the imaged region remains largely disordered, and the interface becomes even less sharp (Figure 3c). While Ni_{0.50}Co_{0.50}O

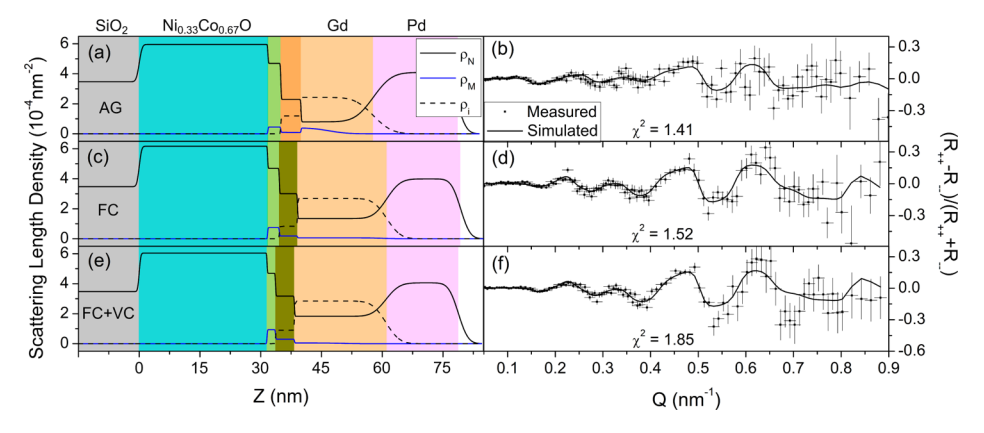


Figure 5. Nuclear and magnetic depth profiles of the $Gd/Ni_{0.33}Co_{0.67}O$ sample in the (a) AG, (c) FC, and (e) FC + VC states, showing the real (ρ_N) , imaginary (ρ_i) , and magnetic (ρ_M) components of the nuclear SLD with a black solid curve, a black dashed curve, and a blue solid curve, respectively. Colored regions are used to indicate various modeled layers: SiO_2 (gray), $Ni_{0.33}Co_{0.67}O$ (teal), NiCo (light green), GdO_x (dark orange), GdN_i (dark green), GdN_i (dark green), GdN_i (magenta), and air (white). The corresponding measured spin asymmetries and the fits for the accepted models are shown in (b), (d), and (f), respectively.

grains are visible in the AG and FC samples, none is visible in the FC + VC sample. Since ionic diffusion is expected to be enhanced at grain boundaries, $^{43-45}$ the disruption of the Ni_{0.50}Co_{0.50}O grains is likely responsible for the irreversibility of the VC effects under a reverse bias.

Elemental distributions of Co (cyan), Ni (pink), Gd (darkblue), and O (green) across the Gd/Ni_{0.50}Co_{0.50}O interface were further obtained by using electron energy loss spectroscopy (EELS) elemental mapping for the AG, FC, and FC + VC states, as shown in Figure 4, with the Gd layer shown at the left end and Ni_{0.50}Co_{0.50}O at the right end. In the AG sample, a weak oxygen signal is observed in the Gd region, suggesting partial oxidation of Gd. A clear Ni and Co region, free of oxygen, is observed at the Gd/Ni_{0.50}Co_{0.50}O interface (Figure 4a), in agreement with magnetometry results. These observations therefore constitute a direct confirmation of the presence of the NiCo metallic layer proposed previously, 12 which is expected to form as a result of Gd-induced oxygen leaching. The oxygen signal is recovered more in the Ni and Co regions (right side), as expected for the Ni_{0.50}Co_{0.50}O layer. In the FC state, the oxygen concentration remains low at the interface. A clear broadening of the oxygen-free Ni and Co interface is observed, along with a partial overlap between Gd and Ni. The latter chemical segregation arises as a result of the lower alloying enthalpy of formation of Gd-Ni alloys as compared to Gd-Co alloys. 46,47 During the initial FC, oxygen migration from Ni_{0.50}Co_{0.50}O to the Gd layer leaves behind metallic NiCo; as a result of Gd-Ni alloys being energetically favored over Gd-Co, the Ni atoms are drawn deeper into the Gd layer and away from the remaining NiCoO layer, accounting for the Ni enrichment near the interface. Additionally, the oxygen concentration decreases in the Gd layer near the interface, suggesting that oxygen has penetrated deeper into the bulk of Gd (Figure 4b). Upon VC, further segregation between the Ni and Co elemental distributions is observed beyond that observed after FC (Figure 4c). In this case, however, the interfacial layer right next to Gd is almost entirely composed of Ni, again pointing to the formation of a Gd-Ni alloy and suggesting that the disorder induced by ionic migration under VC acts to further enhance the chemical segregation effect. Once again, oxygen is absent at the interface and its presence is only significant deep into the NiCoO layer.

Polarized Neutron Reflectometry. Structural and magnetic depth profiles of series 2 samples have been further analyzed by PNR over macroscopic areas, 48,49 as shown in Figure 5a,c,e in terms of the real (ρ_N) and imaginary components (ρ_i) of the nuclear scattering length density (SLD) and the magnetic SLD (ρ_M) . The Gd layer, a strong neutron absorber, is easy to identify during modeling due to its large ρ_i . In addition, O^{2-} migration into Gd can be tracked with increases in ρ_N and decreases in ρ_i with the formation of GdO_x . For all the measured samples (AG, FC, and FC + VC), it was determined that an FM interfacial layer must be present, in agreement with magnetometry results discussed above (Figure 2), as highlighted by the fitted reflectivity (Supporting Information, Figure S1) and spin asymmetry results (Figure 5b,d,f).

In the AG sample, PNR reveals an interfacial NiCo layer between the NiCoO and Gd (Supporting Information, Figure S2). The thickness of the NiCo layer is modeled to be 3.2 nm and exhibits a ρ_N that matches the expected value of 4.7×10^{-4} nm⁻², calculated from a 2:1 composition of Co/Ni at the interface (Figure 5a). The measured magnetic SLD, $\rho_{\rm M}$, of 0.45 \times 10⁻⁴ nm⁻² is smaller than the theoretical value of 3.17 \times 10⁻⁴ nm⁻². The apparently slightly thicker NiCo layer than that observed in STEM and expected from magnetometry, along with the smaller value of $\rho_{\rm M}$, can be attributed to the presence of a discontinuous, non-uniform interfacial NiCo layer with non-FM regions. Adjacent to the NiCo interface is a GdO_x layer with a negligible ρ_M , which can be distinguished from the Gd layer in the ρ_N and ρ_i values. In the Gd layer, ρ_N and ρ_i were best modeled using a continuous value throughout the layer thickness, with increased interface roughness between Gd and Pd. A non-zero $\rho_{\rm M}$ is observed and is attributed to the measurement temperature being near Gd T_C and strain effects (Supporting Information).

For the FC sample, PNR reveals a thinner 2.9 nm NiCo layer at the NiCoO/Gd interface, with a higher $\rho_{\rm M}$ of 0.75 \times 10⁻⁴ nm⁻² (Figure 5c), suggesting a more compact NiCo layer compared to that in the AG sample. Additionally, there is a second interfacial FM layer, differentiable from the GdO_x layer in the AG sample by an increase in $\rho_{\rm N}$, dramatic decrease in $\rho_{\rm i}$, and inclusion of a $\rho_{\rm M}$ corresponding to Ni migration and formation of a Gd–Ni alloy of 4.5 nm. Over much of the Gd layer, the homogeneous $\rho_{\rm i}$ and $\rho_{\rm N}$ distribution suggest that the

FC process may have promoted a redistribution of oxygen along the entire Gd film, evidenced by an increase in ρ_N from $0.80 \times 10^{-4} \text{ nm}^{-2}$ to $1.35 \times 10^{-4} \text{ nm}^{-2}$. For the FC + VC sample, the interfacial NiCo layer thickness is further reduced to 2.1 nm, with a $\rho_{\rm M}$ of 0.94 \times 10⁻⁴ nm⁻². The second interface of the Gd-Ni alloy increases in thickness up to 4.7 nm and ρ_N also increases, indicating further Ni alloying with Gd after VC (Figure 5e). In the Gd layer, a further increase in oxygen content is apparent with an increase in ρ_N to 1.83 \times 10⁻⁴ nm⁻², consistent with the direction of O² migration under voltage application. Note that depth profiles with a single FM layer of NiCo and without the GdNi layer, were also studied, which did not show good fits (Supporting Information, Figures S3 and S4).

DISCUSSION

The observed magnetic behavior of the Gd/Ni_{1-x}Co_xO system is the result of two separate ion migration mechanisms. The first occurs upon the Gd layer deposition, resulting in a chemically induced redox reaction that strips oxygen from the adjacent NiCoO and leaves behind the FM NiCo observed in the magnetometry, PNR, and STEM of the as-grown samples. The resultant valence change at the interface is similar to those reported earlier. 21,24 More disorder is induced at the NiCoO top surface after the Gd deposition (Supporting Information Figure S5). This gadolinium oxidation process is exothermic, with a change in enthalpy ΔH of -11.4 eV per molecule of Gd_2O_3 formed $[3(Ni, Co)O + 2Gd \rightarrow 3(Ni, Co) + Gd_2O_3]^{.50}$ Thus, local heating may help to increase ionic mobility in the surrounding region, although the degree to which this feedback effect enhances the redox reaction is difficult to quantify due to the inhomogeneity of the interface. The magnetization of this structurally disordered interfacial NiCo region is lower than expected for a nominal NiCo alloy, as confirmed by the lower $\rho_{\rm M}$ value extracted from PNR (Figure 3a), owing to the residual oxygen content and different atomic coordinations as compared to the crystalline phase. After the FC process, the enhanced ionic mobility associated with elevated temperatures combined with the Gd-driven chemical potential gradient induces additional oxygen migration beyond that of the AG state and further broadens the interfacial region, as observed in the STEM image.

The second ion migration mechanism is the electric fieldinduced motion. During VC, oxygen ions migrate toward the Gd layer, acting to mix and further disorder the interfacial region. Consequently, the NiCo alloy becomes increasingly Nienriched via the alloying-enthalpy mechanism discussed earlier. As the relative ratio of Ni $(M_s = 495 \text{ emu/cm}^3)$ to Co $(M_s = 1400 \text{ emu/cm}^3)^{36}$ increases, the magnetization of the interfacial layer decreases below that of the FC state. Additionally, the thickness of this layer may also change as a result of the introduction of structural disorder. A number of microscopic accounts of the exchange bias, such as the random field model, 51,52 show that the observed exchange bias is inversely proportional to both the saturation magnetization and the thickness of the FM layer:

$$H_{\rm E} = \frac{2z\sqrt{AK}}{\pi^2 M_{\rm s} t} \tag{1}$$

where A and K are the AF layer exchange stiffness and anisotropy, respectively; M_s and t are the FM saturation magnetization and thickness, respectively; and z is the number

of order unity which depends on the shape of the AF domains. The increase in the bias observed in the hysteresis loops of the FC and FC + VC states suggests that the quantity $M_s t_1^{53}$ which corresponds to the saturation magnetization and the thickness of the FM NiCo at the interface, decreases as a result of VC. This may be due to a decrease in M_s from Ni enrichment or a decrease in the effective FM layer thickness as oxygen migration through the interfacial FM layer alters the structure. This oxygen migration away from NiCoO likely also leads to an increase in the density of pinned uncompensated AF spins at the FM/AF interface, which directly relates to the exchange bias.⁵⁴ These effects act to increase the exchange bias field, in agreement with the measured hysteresis loops of the FC and FC + VC states for both sets of samples.

One possible explanation for the reversibility of the fieldinduced exchange bias enhancement through FC but not reverse bias points to the relative ionic diffusivities along grain boundaries and through the bulk. At room temperature, diffusion along grain boundaries is typically energetically favored over other pathways; 43 at elevated temperatures, bulk diffusion becomes important, and both the bulk and grain boundary diffusivities converge. Upon FC of a pristine sample, the elevated temperatures reached during the thermal cycling are therefore expected to enhance both diffusivities, allowing oxygen migration from Ni_{1-x}Co_xO toward the Gd from the bulk as well as along grain boundaries. The ionic migrations act to disorder Ni_{1-x}Co_xO near its interface with Gd, as can be seen in Figure 4b, but does not fully disrupt the Ni_{1-x}Co_xO/ Gd grain boundaries, which are still visible in the image. The subsequent room-temperature VC conditioning, however, is expected to induce ionic migration primarily along grain boundaries; thus, most disruptions and disordering due to ionic migration are expected at the grain boundaries. Indeed, in the FC + VC STEM image (Figure 3c), only a few crystalline planes are observed over nanometer scale regions whose boundaries are highly disordered. Since ion mobility is expected to be the highest along these grain boundary pathways, disruption to these pathways renders the ionic distributions immobile under a reverse bias, meaning that voltage biasing in this material may be expected to only cause significant ionic migration under the first VC treatment. Importantly, a second FC procedure can reset the exchange bias back to its original value. Since bulk ionic diffusivity is enhanced at elevated temperatures, grain boundaries are not as important for ionic migration during FC, allowing the interface to recover to the pre-voltage-conditioned state.

CONCLUSIONS

In summary, effective magneto-ionic control and electric field enhancement of the exchange bias in Ni_{1-x}Co_xO/Gd have been demonstrated. Ferromagnetism emerges in this system, featuring constituents that are not FM at room temperature, due to the formation of a NiCo layer at the Ni_{1-r}Co_rO/Gd interface. This FM layer is observed by magnetometry and PNR and is directly confirmed by EELS. This is the result of oxygen ion migration induced by a Gd-oxidation reaction. An exchange bias is established via a field cooling process, which can be further enhanced up to 35% under an electric field gating. EELS and PNR results confirm that upon field cooling, the interfacial NiCo region becomes broader and Ni-rich. Upon voltage conditioning, the reduction of the interfacial NiCo moment due to the additional formation of the GdNi alloy and disorder-induced changes to the effective thickness of the FM layer and the density of pinned uncompensated AF spins contribute to the enhancement of the exchange bias. Finally, this effect was found to be reversible under thermal cycling but not under reverse biasing due to ionic-migration-induced disruption of grain boundaries near the interface, which comprise the most effective pathways for ionic motion. These results demonstrate a new magneto-ionic approach toward electric manipulation of the exchange bias, which is highly relevant for energy-efficient spintronic devices.

ASSOCIATED CONTENT

Supporting Information

The Supporting Information is available free of charge at https://pubs.acs.org/doi/10.1021/acsami.1c11126.

Methods, PNR measurements of the $Gd/Ni_{0.33}Co_{0.67}O$ samples in AG, FC, and FC + VC states, and X-ray reflectivity measurements (PDF)

AUTHOR INFORMATION

Corresponding Author

Kai Liu — Physics Department, Georgetown University, Washington, District of Columbia 20057, United States; Physics Department, University of California, Davis, California 95616, United States; ⊚ orcid.org/0000-0001-9413-6782; Email: Kai.Liu@georgetown.edu

Authors

Peyton D. Murray — Physics Department, University of California, Davis, California 95616, United States;
ocid.org/0000-0003-0389-0611

Christopher J. Jensen — Physics Department, Georgetown University, Washington, District of Columbia 20057, United States; occid.org/0000-0001-7459-1841

Alberto Quintana — Physics Department, Georgetown University, Washington, District of Columbia 20057, United States; orcid.org/0000-0002-9813-735X

Junwei Zhang – King Abdullah University of Science & Technology, Thuwal 23955-6900, Saudi Arabia

Xixiang Zhang — King Abdullah University of Science & Technology, Thuwal 23955-6900, Saudi Arabia; orcid.org/0000-0002-3478-6414

Alexander J. Grutter — NIST Center for Neutron Research, National Institute of Standards and Technology, Gaithersburg, Maryland 20899, United States; Ocid.org/ 0000-0002-6876-7625

Brian J. Kirby — NIST Center for Neutron Research, National Institute of Standards and Technology, Gaithersburg, Maryland 20899, United States

Complete contact information is available at: https://pubs.acs.org/10.1021/acsami.1c11126

Notes

The authors declare no competing financial interest.

■ ACKNOWLEDGMENTS

This work was supported in part by the NSF (ECCS-1611424 and ECCS-1933527), by SMART, one of the seven centers of nCORE, a Semiconductor Research Corporation program, sponsored by the National Institute of Standards and Technology (NIST), and by KAUST (OSR-2019-CRG8-4081). The acquisition of a Magnetic Property Measurements System (MPMS3) at GU which was used in this investigation

was supported by the NSF (DMR-1828420). We thank Professor Yayoi Takamura for helpful discussions.

REFERENCES

- (1) Ohno, H.; Chiba, D.; Matsukura, F.; Omiya, T.; Abe, E.; Dietl, T.; Ohno, Y.; Ohtani, K. Electric-Field Control of Ferromagnetism. *Nature* **2000**, *408*, 944–946.
- (2) Weisheit, M.; Fahler, S.; Marty, A.; Souche, Y.; Poinsignon, C.; Givord, D. Electric Field-Induced Modification of Magnetism in Thin-Film Ferromagnets. *Science* **2007**, *315*, 349–351.
- (3) Chu, Y.-H.; Martin, L. W.; Holcomb, M. B.; Gajek, M.; Han, S.-J.; He, Q.; Balke, N.; Yang, C.-H.; Lee, D.; Hu, W.; Zhan, Q.; Yang, P.-L.; Fraile-Rodríguez, A.; Scholl, A.; Wang, S. X.; Ramesh, R. Electric-Field Control of Local Ferromagnetism using a Magneto-electric Multiferroic. *Nat. Mater.* **2008**, *7*, 478–482.
- (4) Chiba, D.; Fukami, S.; Shimamura, K.; Ishiwata, N.; Kobayashi, K.; Ono, T. Electrical control of the ferromagnetic phase transition in cobalt at room temperature. *Nat. Mater.* **2011**, *10*, 853–856.
- (5) Wang, W.-G.; Li, M.; Hageman, S.; Chien, C. L. Electric-Field-Assisted Switching in Magnetic Tunnel Junctions. *Nat. Mater.* **2012**, 11. 64–68.
- (6) Bauer, U.; Emori, S.; Beach, G. S. D. Voltage-Controlled Domain Wall Traps in Ferromagnetic Nanowires. *Nat. Nanotechnol.* **2013**, *8*, 411–416.
- (7) Bi, C.; Liu, Y.; Newhouse-Illige, T.; Xu, M.; Rosales, M.; Freeland, J. W.; Mryasov, O.; Zhang, S.; te Velthuis, S. G. E.; Wang, W. G. Reversible Control of Co Magnetism by Voltage-Induced Oxidation. *Phys. Rev. Lett.* **2014**, *113*, 267202.
- (8) Bauer, U.; Yao, L.; Tan, A. J.; Agrawal, P.; Emori, S.; Tuller, H. L.; van Dijken, S.; Beach, G. S. D. Magneto-Ionic Control of Interfacial Magnetism. *Nat. Mater.* **2015**, *14*, 174–181.
- (9) Gilbert, D. A.; Grutter, A. J.; Arenholz, E.; Liu, K.; Kirby, B. J.; Borchers, J. A.; Maranville, B. B. Structural and Magnetic Depth Profiles of Magneto-Ionic Heterostructures Beyond the Interface Limit. *Nat. Commun.* **2016**, *7*, 12264.
- (10) Nakano, M.; Shibuya, K.; Okuyama, D.; Hatano, T.; Ono, S.; Kawasaki, M.; Iwasa, Y.; Tokura, Y. Collective Bulk Carrier Delocalization Driven by Electrostatic Surface Charge Accumulation. *Nature* **2012**, *487*, 459–462.
- (11) Jeong, J.; Aetukuri, N.; Graf, T.; Schladt, T. D.; Samant, M. G.; Parkin, S. S. P. Suppression of Metal-Insulator Transition in VO2 by Electric Field-Induced Oxygen Vacancy Formation. *Science* **2013**, 339, 1402–1405.
- (12) Gilbert, D. A.; Olamit, J.; Dumas, R. K.; Kirby, B. J.; Grutter, A. J.; Maranville, B. B.; Arenholz, E.; Borchers, J. A.; Liu, K. Controllable Positive Exchange Bias via Redox-Driven Oxygen Migration. *Nat. Commun.* **2016**, *7*, 11050.
- (13) Tan, A. J.; Huang, M.; Avci, C. O.; Büttner, F.; Mann, M.; Hu, W.; Mazzoli, C.; Wilkins, S.; Tuller, H. L.; Beach, G. S. D. Magneto-Ionic Control of Magnetism using a Solid-State Proton Pump. *Nat. Mater.* **2019**, *18*, 35–41.
- (14) Walter, J.; Wang, H.; Luo, B.; Frisbie, C. D.; Leighton, C. Electrostatic versus Electrochemical Doping and Control of Ferromagnetism in Ion-Gel-Gated Ultrathin La0.5Sr0.5CoO3 $-\delta$. ACS Nano **2016**, 10, 7799.
- (15) Leighton, C. Electrolyte-based Ionic Control of Functional Oxides. *Nat. Mater.* **2019**, *18*, 13–18.
- (16) Zehner, J.; Huhnstock, R.; Oswald, S.; Wolff, U.; Soldatov, I.; Ehresmann, A.; Nielsch, K.; Holzinger, D.; Leistner, K. Nonvolatile Electric Control of Exchange Bias by a Redox Transformation of the Ferromagnetic Layer. *Adv. Electron. Mater.* **2019**, *5*, 1900296.
- (17) Navarro-Senent, C.; Quintana, A.; Menéndez, E.; Pellicer, E.; Sort, J. Electrolyte-Gated Magnetoelectric Actuation: Phenomenology, Materials, Mechanisms, and Prospective Applications. *APL Mater.* **2019**, *7*, 030701.
- (18) Walter, J.; Voigt, B.; Day-Roberts, E.; Heltemes, K.; Fernandes, R. M.; Birol, T.; Leighton, C. Voltage-Induced Ferromagnetism in a Diamagnet. *Sci. Adv.* **2020**, *6*, No. eabb7721.

- (19) Nichterwitz, M.; Honnali, S.; Kutuzau, M.; Guo, S.; Zehner, J.; Nielsch, K.; Leistner, K. Advances in Magneto-Ionic Materials and Perspectives for Their Application. *APL Mater.* **2021**, *9*, 030903.
- (20) Gu, Y.; Song, C.; Wang, Q.; Hu, W.; Liu, W.; Pan, F.; Zhang, Z. Emerging Opportunities for Voltage-Driven Magneto-Ionic Control in Ferroic Heterostructures. *APL Mater.* **2021**, *9*, 040904.
- (21) Gilbert, D. A.; Grutter, A. J.; Murray, P. D.; Chopdekar, R. V.; Kane, A. M.; Ionin, A. L.; Lee, M. S.; Spurgeon, S. R.; Kirby, B. J.; Maranville, B. B.; N'Diaye, A. T.; Mehta, A.; Arenholz, E.; Liu, K.; Takamura, Y.; Borchers, J. A. Ionic Tuning of Cobaltites at the Nanoscale. *Phys. Rev. Mater.* **2018**, 2, 104402.
- (22) Quintana, A.; Menéndez, E.; Liedke, M. O.; Butterling, M.; Wagner, A.; Sireus, V.; Torruella, P.; Estradé, S.; Peiró, F.; Dendooven, J.; Detavernier, C.; Murray, P. D.; Gilbert, D. A.; Liu, K.; Pellicer, E.; Nogues, J.; Sort, J. Voltage-Controlled ON-OFF Ferromagnetism at Room Temperature in a Single Metal Oxide Film. *ACS Nano* 2018, 12, 10291–10300.
- (23) de Rojas, J.; Quintana, A.; Lopeandía, A.; Salguero, J.; Muñiz, B.; Ibrahim, F.; Chshiev, M.; Nicolenco, A.; Liedke, M. O.; Butterling, M.; Wagner, A.; Sireus, V.; Abad, L.; Jensen, C. J.; Liu, K.; Nogués, J.; Costa-Krämer, J. L.; Menéndez, E.; Sort, J. Voltage-Driven Motion of Nitrogen Ions: A New Paradigm for Magneto-Ionics. *Nat. Commun.* **2020**, *11*, 5871.
- (24) Murray, P. D.; Gilbert, D. A.; Grutter, A. J.; Kirby, B. J.; Hernández-Maldonado, D.; Varela, M.; Brubaker, Z. E.; Liyanage, W. L. N. C.; Chopdekar, R. V.; Taufour, V.; Zieve, R. J.; Jeffries, J. R.; Arenholz, E.; Takamura, Y.; Borchers, J. A.; Liu, K. Interfacial-Redox-Induced Tuning of Superconductivity in YBa2Cu3O7-δ. ACS Appl. Mater. Interfaces 2020, 12, 4741–4748.
- (25) Perez-Muñoz, A. M.; Schio, P.; Poloni, R.; Fernandez-Martinez, A.; Rivera-Calzada, A.; Cezar, J. C.; Salas-Colera, E.; Castro, G. R.; Kinney, J.; Leon, C.; Santamaria, J.; Garcia-Barriocanal, J.; Goldman, A. M. Operando Evidence of Deoxygenation in Ionic Liquid Gating of YBa₂Cu₃O_{7-X}. *Proc. Natl. Acad. Sci. U.S.A.* **2017**, *114*, 215.
- (26) Chen, G.; Mascaraque, A.; Jia, H.; Zimmermann, B.; Robertson, M.; Conte, R. L.; Hoffmann, M.; González Barrio, M. A.; Ding, H.; Wiesendanger, R.; Michel, E. G.; Blügel, S.; Schmid, A. K.; Liu, K. Large Dzyaloshinskii-Moriya Interaction Induced by Chemisorbed Oxygen on a Ferromagnet Surface. Sci. Adv. 2020, 6, No. eaba4924.
- (27) Chen, G.; Robertson, M.; Hoffmann, M.; Ophus, C.; Cauduro, A. L. F.; Lo Conte, R.; Ding, H. F.; Wiesendanger, R.; Blügel, S.; Schmid, A. K.; Liu, K. Observation of Hydrogen-Induced Dzyaloshinskii-Moriya Interaction and Reversible Switching of Magnetic Chirality. *Phys. Rev. X* **2021**, *11*, 021015.
- (28) Diez, L. H.; Liu, Y. T.; Gilbert, D. A.; Belmeguenai, M.; Vogel, J.; Pizzini, S.; Martinez, E.; Lamperti, A.; Mohammedi, J. B.; Laborieux, A.; Roussigné, Y.; Grutter, A. J.; Arenholtz, E.; Quarterman, P.; Maranville, B.; Ono, S.; Hadri, M. S. E.; Tolley, R.; Fullerton, E. E.; Sanchez-Tejerina, L.; Stashkevich, A.; Chérif, S. M.; Kent, A. D.; Querlioz, D.; Langer, J.; Ocker, B.; Ravelosona, D. Nonvolatile Ionic Modification of the Dzyaloshinskii-Moriya Interaction. *Phys. Rev. Appl.* **2019**, *12*, 034005.
- (29) Grutter, A. J.; Gilbert, D. A.; Alaan, U. S.; Arenholz, E.; Maranville, B. B.; Borchers, J. A.; Suzuki, Y.; Liu, K.; Kirby, B. J. Reversible Control of Magnetism in La_{0.67}Sr_{0.33}MnO₃ through Chemically-Induced Oxygen Migration. *Appl. Phys. Lett.* **2016**, *108*, 082405.
- (30) Nogués, J.; Schuller, I. K. Exchange Bias. J. Magn. Magn. Mater. 1999, 192, 203–232.
- (31) Kiwi, M. Exchange Bias Theory. J. Magn. Magn. Mater. 2001, 234, 584-595.
- (32) Berkowitz, A. E.; Takano, K. Exchange Anisotropy. *J. Magn. Magn. Mater.* **1999**, 200, 552–570.
- (33) He, X.; Wang, Y.; Wu, N.; Caruso, A. N.; Vescovo, E.; Belashchenko, K. D.; Dowben, P. A.; Binek, C. Robust Isothermal Electric Control of Exchange Bias at Room Temperature. *Nat. Mater.* **2010**, *9*, 579–585.
- (34) Manipatruni, S.; Nikonov, D. E.; Lin, C.-C.; Prasad, B.; Huang, Y.-L.; Damodaran, A. R.; Chen, Z.; Ramesh, R.; Young, I. A. Voltage

- Control of Unidirectional Anisotropy in Ferromagnet-Multiferroic System. Sci. Adv. 2018, 4, No. eaat4229.
- (35) Wei, L.; Hu, Z.; Du, G.; Yuan, Y.; Wang, J.; Tu, H.; You, B.; Zhou, S.; Qu, J.; Liu, H.; Zheng, R.; Hu, Y.; Du, J. Full Electric Control of Exchange Bias at Room Temperature by Resistive Switching. *Adv. Mater.* **2018**, *30*, 1801885.
- (36) Kittel, C. Introduction to Solid State Physics, 8th ed.; Wiley: Hoboken, NJ, 2005.
- (37) Takano, M.; Terashima, T.; Bando, Y.; Ikeda, H. Neutron Diffraction Study of Artificial CoO-NiO Superlattices. *Appl. Phys. Lett.* **1987**, *51*, 205–206.
- (38) Ambrose, T.; Liu, K.; Chien, C. L. Doubly Exchange-Biased NiCoO/NiFe/Cu/NiFe/NiCoO Spin Valves. *J. Appl. Phys.* **1999**, *85*, 6124.
- (39) Estrada, W.; Andersson, A. M.; Granqvist, C. G. Electrochromic Nickel-Oxide-Based Coatings Made by Reactive DC Magnetron Sputtering: Preparation and Optical Properties. *J. Appl. Phys.* **1988**, 64, 3678–3683.
- (40) Yi, J. Y.; Platt, C. L.; Rudee, M. L.; Berkowitz, A. E.; Cheeks, T. L. Sputter Deposited Co/CoO Composite Materials. *J. Appl. Phys.* **1996**, *79*, 5072.
- (41) Carey, M. J.; Spada, F. E.; Berkowitz, A. E.; Cao, W.; Thomas, G. Preparation and Structural Characterization of Sputtered CoO, NiO, and Ni_{0.5}Co_{0.5}O Thin Epitaxial Films. *J. Mater. Res.* **2011**, *6*, 2680–2687.
- (42) Carey, M. J.; Berkowitz, A. E. Exchange Anisotropy in Coupled Films of Ni₈₁Fe₁₉ with NiO and Co_xNi_{1-x}O. *Appl. Phys. Lett.* **1992**, *60*, 3060–3062.
- (43) Balluffi, R. W. Kinetics of Materials; John Wiley & Sons: Hoboken, N.J, 2005.
- (44) Hotovy, I.; Liday, J.; Spiess, L.; Sitter, H.; Vogrincic, P. Study of Annealed NiO Thin Films Sputtered on Unheated Substrate. *Jpn. J. Appl. Phys.* **2003**, *42*, L1178–L1181.
- (45) Kim, Y.-M.; He, J.; Biegalski, M. D.; Ambaye, H.; Lauter, V.; Christen, H. M.; Pantelides, S. T.; Pennycook, S. J.; Kalinin, S. V.; Borisevich, A. Y. Probing Oxygen Vacancy Concentration and Homogeneity in Solid-Oxide Fuel-Cell Cathode Materials on the Subunit-Cell Level. *Nat. Mater.* 2012, 11, 888–894.
- (46) Colinet, C.; Pasturel, A.; Buschow, K. H. J. Study of the Enthalpies of Formation in the Gd-Ni System. *Metall. Trans. A* **1986**, 17, 777–780.
- (47) Colinet, C.; Pasturel, A.; Buschow, K. H. J. Study of the Enthalpies of Formation in the Gd-(Fe, Co, Pd, Pt) Systems. *Metall. Mater. Trans. A* **1987**, *18*, 903–907.
- (48) Kirby, B. J.; Kienzle, P. A.; Maranville, B. B.; Berk, N. F.; Krycka, J.; Heinrich, F.; Majkrzak, C. F. Phase-Sensitive Specular Neutron Reflectometry for Imaging the Nanometer Scale Composition Depth Profile of Thin-Film Materials. *Curr. Opin. Colloid Interface Sci.* 2012, 17, 44–53.
- (49) Maranville, B.; Ratcliff II, W., II; Kienzle, P. Reductus: A Stateless Python Data Reduction Service with a Browser Front End. *J. Appl. Crystallogr.* **2018**, *51*, 1500–1506.
- (50) Dean, J. A. Lange's Handbook of Chemistry, 17th ed.; McGraw-Hill Professional, 2017.
- (51) Malozemoff, A. P. Random-Field Model of Exchange Anisotropy at Rough Ferromagnetic-Antiferromagnetic Interfaces. *Phys. Rev. B* **1987**, *35*, 3679–3682.
- (52) Li, Z.; Zhang, S. F. Coercive Mechanisms in Ferromagnetic-Antiferromagnetic Bilayers. *Phys. Rev. B* **2000**, *611*, 14897.
- (53) Zhou, S. M.; Liu, K.; Chien, C. L. Exchange Coupling and Macroscopic Domain Structure in a Wedged Permalloy/FeMn Bilayer. *Phys. Rev. B* **1998**, *58*, R14717.
- (54) Ohldag, H.; Scholl, A.; Nolting, F.; Arenholz, E.; Maat, S.; Young, A. T.; Carey, M.; Stöhr, J. Correlation Between Exchange Bias and Pinned Interfacial Spins. *Phys. Rev. Lett.* **2003**, *91*, 017203.